Hindawi Publishing Corporation
Journal of Nanomaterials
Volume 2016, Article ID 2629582, 8 pages
http://dx.doi.org/10.1155/2016/2629582

Research Article

Surface Functionality Features of Porous Silicon Prepared and Treated in Different Conditions

Yu. M. Spivak,[1] S. V. Mjakin,[2] V. A. Moshnikov,[1] M. F. Panov,[1] A. O. Belorus,[1] and A. A. Bobkov[1]

[1]*Department of Micro- and Nanoelectronics, Saint Petersburg Electrotechnical University "LETI", 5 Professor Popova Street, Saint Petersburg 197376, Russia*
[2]*Department of Theory of Materials Science, Saint Petersburg State Technological Institute (Technical University), 26 Moskovsky Prospect, Saint Petersburg 190013, Russia*

Correspondence should be addressed to Yu. M. Spivak; ymspivak@etu.ru

Received 10 December 2015; Revised 10 March 2016; Accepted 13 March 2016

Academic Editor: Mahaveer Kurkuri

Hydrophilic layers of porous silicon are prepared by single- or two-step anodization and characterized by evaluating their surface hydrophilicity and contents of functional groups using IR spectroscopy and adsorption of acid-base indicators with different pK_a values. The surface functional composition of the synthesized samples is shown to be adjustable depending on the anodization current density. The surface of samples obtained at anodization current density 30 mA/cm^2 is predominantly occupied with pK_a 2.5 corresponding to ≡Si–OH groups. The increase of current density to 80 mA/cm^2 results in the increase of surface functional nonuniformity with the formation of versatile centers, primarily Lewis acidic sites corresponding to Si atoms, as indicated by selective indicator adsorption in agreement with the disappearance of Si–H bonds in IR spectra and overall surface disordering according to SEM and AFM data.

1. Introduction

Porous silicon (por-Si) is a promising material for sensors, biosensors, and specific medical purposes [1–4]. Biomedical applications of por-Si involve the use as a carrier for target delivery of single or combined drugs [5–9], photosensitive agents in photodynamic therapy and in tissue engineering [10], various biodetectors, and biomedical imaging [11] including tumor visualization, as well as eye diseases. Modified por-Si layers can be used in biosensors [1, 2, 4, 12–17] for various applications including the determination of glucose, DNA, antibodies, bacteria, and viruses [12–14]. This application area involves different types of sensors, including electric, electrochemical, optical, and labeling devices [15–17]. Biosensor application of por-Si also includes the use in passive platforms for the deposition of biological cultures and active elements interaction with the biological environment [15, 18, 19]. A highly developed porous structure of por-Si facilitates the development of highly efficient parallel biochips for the analysis of several cultures in one platform. Furthermore, por-Si is a promising material for nanocontainers in targeted drug delivery [3–9, 20]. The main advantages of por-Si nanocontainers include high sorption or carrier capacity due to a large surface area, pore volume and concentration, high stability, biocompatibility, versatility of modifications and characteristics, inexpensive synthesis processes, and easy exploration in target applications [4, 9, 20–23]. Moreover, por-Si nanocontainers are efficient for *in vivo* applications since they dissolve in an organism with the rate adjustable by varying the porosity and surface chemistry [4, 24–26] and yield only a nontoxic orthosilicic acid that affords a controllable drug release from such nanocontainers.

In this way, por-Si nanoparticles can be used for effective delivery of antiviral drugs to infected cells. In [27] a significant increase of Streptocidum (saliphenylhalamide, SaliPhe) solubility was achieved by encapsulating this antibiotic into thermally hydrocarbonized por-Si (THCPSi) nanoparticles subsequently releasing this drug to inhibit influenza infection

in vitro and reduce the number of progeny viruses in influenza-infected cells. In addition to increased solubility, the considered por-Si based nanosystems were shown to provide improved drug delivery properties, including high stability *in vitro* and low cytotoxicity [27]. The preparation of biodegradable por-Si nanoparticles functionalized with antibodies that target cancer cells and containing a hydrophobic anticancer drug camptothecin described in [7] afforded a successful targeting and selective destruction of cancer cells.

A highly promising application area relates to the development of systems for a simultaneous delivery of different therapeutic agents, for example, low molecular weight drugs, and with relatively large peptides [6], such as hydrophobic indomethacin in combination with hydrophilic human peptide YY3-36 (PYY3-36). The authors argue that the startup sequence of the two drugs in por-Si nanoparticles affects the release rate of each drug. PYY3-36 was found to provide a significant improvement of por-Si nanoparticles cytological compatibility and possess a biological activity and ability to penetrate the intestinal cells after the release from nanoparticulate por-Si carrier.

Depending on the type of carried drugs and their chemical composition, particularly specific functional groups (hydroxyl groups, amino groups, etc.) in their molecules, the nanocontainer surface should meet the corresponding requirements such as hydrophilic or hydrophobic nature, presence of certain adsorption centers (functional groups), and charge. By adjusting the technological conditions, it is possible to adjust geometric characteristics of the porous texture and the composition of the porous silicon surface. It is significant for delivering various therapeutic agents, from small drugs to large molecular peptides/protein therapeutics [4]. Particularly, the hydrophilic-hydrophobic, acid-base, and donor-acceptor properties determined by the presence of specific centers and functional groups on the surface significantly affect such properties as wettability, permeability of pores to certain substances (that in turn determines the selection of solvents or dispersion media), and interaction with physiological liquids and drugs.

Furthermore, the phase composition and morphology of porous silicon surface are also highly important. These properties are known to markedly vary depending on the source material and electrochemical processing conditions parameters [9, 20, 21, 28–30]. XANES and IR spectroscopy investigations [29] revealed that the ratio between oxide and silicon phases in the surface layer is higher for por-Si obtained at low-resistance substrates of n-Si compared with p-por-Si samples due to the concentration and type of substrate doping impurities. Furthermore, XANES and XPS studies indicated a considerable variation of por-Si phase composition, particularly the content of α-Si, α-Si : H, and nanocrystalline silicon (nc-Si) phases in depth of the porous layer [21, 30]. The surface layer is enriched with a mixture of silicon dioxide, nonstoichiometric silicon oxide (up to 48%), and hydrogenated amorphous silicon while the percentage of nc-Si grows with depth (e.g., to 62% at the depth of 60 nm).

In addition to the specific composition of functional groups, their general acid-base properties as well as the charge state of por-Si surface are also very important factors that should be considered when choosing the conditions for obtaining porous silicon; they significantly affect the interaction mechanism between por-Si carrier surface and grafted therapeutic agents or other substances.

An effective approach to the study of adsorption centers and functional groups on the surface of solids using a selective adsorption of acid-base indicators with different pK_a values was suggested in [31, 32]. This method is extremely sensitive and allows distinguishing the functional groups of the same chemical composition differing only in the electron density distribution and therefore in their acid-base and donor-acceptor properties characterized by their pK_a values. Earlier the considered technique was successfully applied in the study of various oxide materials [31, 32]; however it was never used in respect of porous silicon.

This research work is aimed at the study of possibilities to control the surface composition of por-Si useful for target drug delivery by the variation of its synthesis parameters via electrochemical anodization in an Unno-Imai cell.

2. Experimental

2.1. Preparation of Porous Silicon Layers. Por-Si layers were prepared by electrochemical anodization of monocrystalline silicon in an Unno-Imai [33]. The application of Unno-Imai method is determined by a more uniform electric field distribution over the anodized sample in the case of a double-chamber cell compared with a single-chamber one due to a direct electric contact between the silicon plate cathode side and electrolyte in the second consecutively connected cell (chamber). This approach provides an increased uniformity of the porous layer characteristics over the plate surface and simplifies the plate preparation for anodization because a preliminary formation of a highly doped or metal layer on the nonprocessed side of the plate is not required in this case.

KEF-5 silicon (111, n-type conductivity, doped with phosphorus, electric resistance 5 Ohm·cm) was used as a source substrate material. All the samples were subjected to the same pretreatment procedures before and posttreatment procedures after the electrochemical anodization.

The electrochemical anodization was carried out using an aqueous electrolyte comprising HF aqueous solution with addition of isopropyl alcohol [4, 34]. Porous silicon was prepared via a single- and two-stage anodization with the variation of current density J and anodization time t. The process conditions are summarized in Table 1.

2.2. Characterization Methods. The morphology and texture of the obtained por-Si samples were characterized by SEM (Phenom) and AFM (Ntegra Terma, NT-MDT) methods.

The composition of functional groups on por-Si surface was studied by FTIR reflectance spectroscopy using a Nicolet-6700 installation in a mode specifically useful for the characterization of semiconductors [4, 21, 29, 35, 36] involving both integrated (over a large surface) and local (in the areas up to 10 μm) ones. This characterization was performed for samples obtained under different conditions in single- and two-phase synthesis as well as for samples prepared under the

Table 1: Conditions of por-Si layers preparation.

Series of samples	Current density J, mA/cm^2	t, min	Number of prepared samples	Notes
I	30	15	8	Single-stage anodization
II	80	15	8	Single-stage anodization
III	Stage 1: 80 Stage 2: 30	Stage 1: 30 Stage 2: 60	2	Two-stage anodization
IV			2	Two-stage anodization, storage in ambient conditions for 2 years

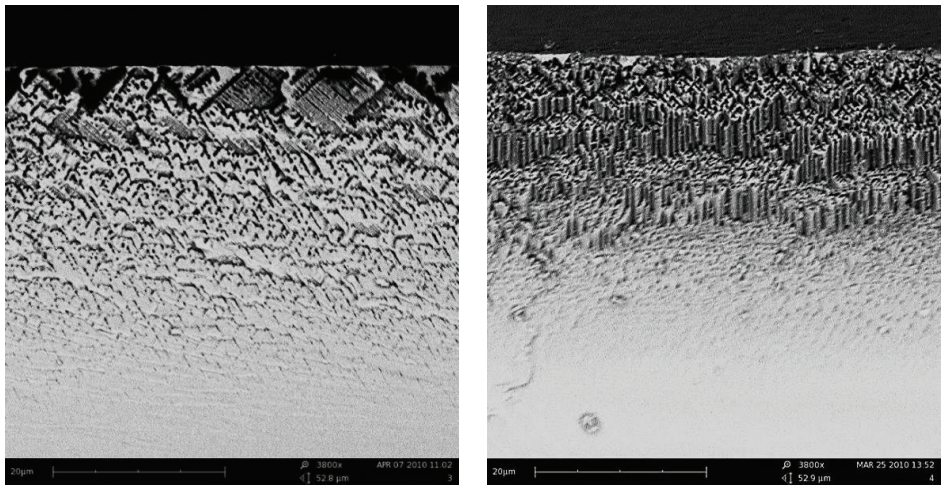

(a) (b)

Figure 1: Texture of obtained por-Si illustrated by SEM data of splits for samples synthesized at (a) $j = 30\,\text{mA/cm}^2$, $t = 60\,\text{min}$ and (b) $j = 80\,\text{mA/cm}^2$, $t = 30\,\text{min}$.

same conditions straight upon the synthesis and after 2-year storage in ambient conditions.

Furthermore, in order to precisely analyze the surface functionality of the samples, they were also studied using a selective adsorption of acid-base indicators with different pK_a values. This method described in detail in [31, 32] affords a highly sensitive determination and distinguishing surface centers, including functional groups of the same chemical composition differing only in the electron density distribution and, consequently, in their acid-base and donor-acceptor properties. In this paper we determined the content of the acid centers on the surface of the synthesized samples: the typical silicon surface Lewis acid centers (Si atoms) and Bronsted acid centers (groups ≡Si–OH), close to the neutral centers (group =Si(OH)$_2$) and the main centers (the group –Si(OH)$_3$).

3. Results and Discussion

3.1. Effect of Synthesis Parameters on por-Si Morphology and Texture. SEM data for splits of por-Si samples prepared under anodization conditions corresponding to each stage of series III separately and after the complete two-stage anodization as well as for a sample synthesized in a single stage within the time equal to the overall anodization time for series III at current density 80 mA/cm^2 are shown in Figures 1 and 2.

The textural characterization of these samples suggests that in the considered conditions a system of channels is formed involving meso- and macropores predominantly spread along a (100) crystallographic direction. The samples prepared at the current density 80 mA/cm^2 are featured with the presence of pores directed rectangularly to the surface plane that probably accounted for the applied electric field geometry and competing processes at anodization.

As shown in Figure 2, two-stage anodization with the variation of current density in the considered conditions provides the formation of two por-Si layers with a well-defined boundary. The textural features of por-Si layers prepared in a two-stage mode (Figure 2(a)) resemble that for the samples synthesized in a single-phase mode in the similar conditions (Figures 1(a) and 1(b)). The formation of more loose and highly developed surface for samples prepared in two stages is probably determined by the second-stage features involving not only the formation of por-Si layer with modified texture during the anodization front movement inside the substrate but also a certain additional etching of the top por-Si layer.

AFM data (Figure 3) indicate that the increase in the anodization current density leads to the increase of the

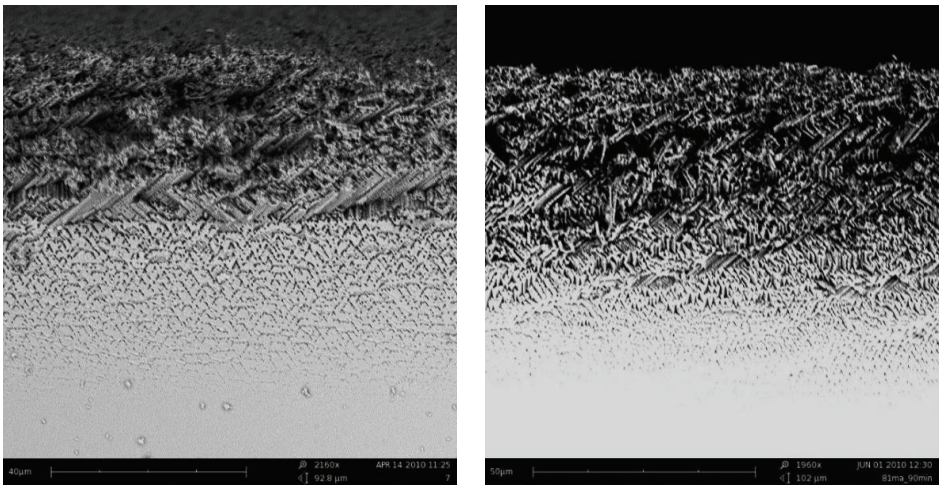

(a) (b)

Figure 2: SEM data for splits of por-Si samples prepared (a) in two-stage (stage 1: $j = 80\,\text{mA/cm}^2$, $t = 30\,\text{min}$; stage 2: $j = 30\,\text{mA/cm}^2$, $t = 60\,\text{min}$) and (b) single-stage anodization ($j = 80\,\text{mA/cm}^2$, $t = 90\,\text{min}$).

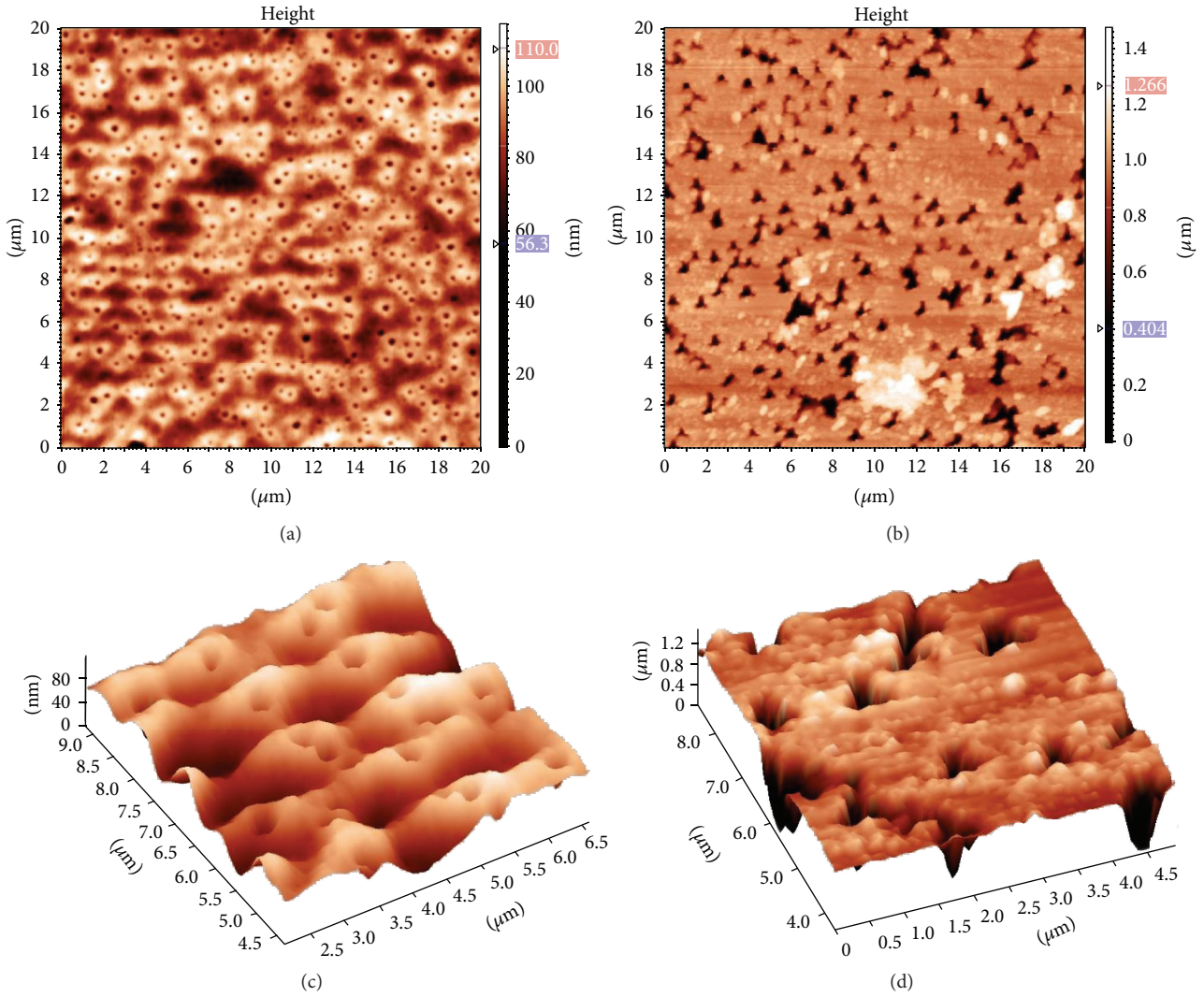

Figure 3: Morphology of por-Si layers according to AFM data: (a), (c) series I ($j = 30\,\text{mA/cm}^2$); (b), (d) series II ($j = 80\,\text{mA/cm}^2$).

resulting pore size and a significant surface flattening between the pores.

3.2. IR Spectroscopy Data on the Composition of Functional Groups on the Surface of Porous Silicon. IR reflectance spectroscopy analyses were carried out for por-Si samples prepared via a single-stage anodization in two different modes: (a) $j = 80\,\text{mA/cm}^2$, $t = 30\,\text{min}$ and (b) $j = 30\,\text{mA/cm}^2$, $t = 60\,\text{min}$, as well as via a two-stage process involving consecutively performed stages (a) and (b). For the latter samples IR spectra were recorded straight upon the synthesis and after 2-year storage in ambient conditions (series III and IV in Table 1, resp.). IR spectra of the studied samples are illustrated in Figures 4 and 5. The observed absorption bands are interpreted in accordance with reference data [29, 37–39] and summarized in Table 2.

The comparative analysis of the considered data indicates the following: IR spectra of all the studied por-Si samples involve absorption bands at 2958, 2927, and $2856\,\text{cm}^{-1}$ suggesting the presence of carbon-containing complexes on their surface. The amount of carbon-containing complexes grows with the increase of anodization current density (Figure 4). According to [36], the appearance of carbon-containing species on por-Si surface is determined by the electrochemical oxidation of an alcohol component of electrolyte yielding C=O groups reacting with surface hydroxyls. The sample obtained in a single stage at $j = 30\,\text{mA/cm}^2$ and $t = 60\,\text{min}$ is featured with a significantly reduced content of such species (among the discussed bands, only peaks at 2927 and $2856\,\text{cm}^{-1}$ corresponding to stretching antisymmetric vibrations of CH– in CH_2 and CH, resp., are present in their spectra) compared with the sample prepared at higher current density. For the sample prepared using a two-stage synthesis their amount is further decreased. These data are in agreement with the conclusions that anodization at the second stage results in the formation of a new por-Si layer inside the silicon plate below the already formed layer (anodization front spreads inside the substrate) and etching of the top layer (Figure 2(a)). The content of nano- and mesopores also drops consequently resulting in the decrease of alcohol and its electrochemical oxidation products.

In the range 3100–$3700\,\text{cm}^{-1}$ a broad absorption band is observed corresponding to surface hydroxyls (O–H bonds). The surface of obtained por-Si samples is featured with hydrophilicity (as suggested by the absence of bands at 948 and $644\,\text{cm}^{-1}$ intrinsic to Si–H bonds in the spectra of samples straight after preparation) mostly prominent in the case of anodization current density $30\,\text{mA/cm}^2$.

The presence of absorption bands numbers 7 and 8 (1056–$1160\,\text{cm}^{-1}$) responsible for antisymmetric stretching vibrations of SiO– in O–SiO and C–SiO is typical for the oxidation of a highly developed surface of por-Si.

2-year storage (samples of the series IV) results in the increase of peaks indicated by number 4 (the most intensive peak in this region corresponding to O_3SiH group) and number 5 ($SiH–SiO_2$ group) that in combination with a high intensity of antisymmetric stretching bands of SiO– in O–SiO and C–SiO probably reflects the oxide layer growth on

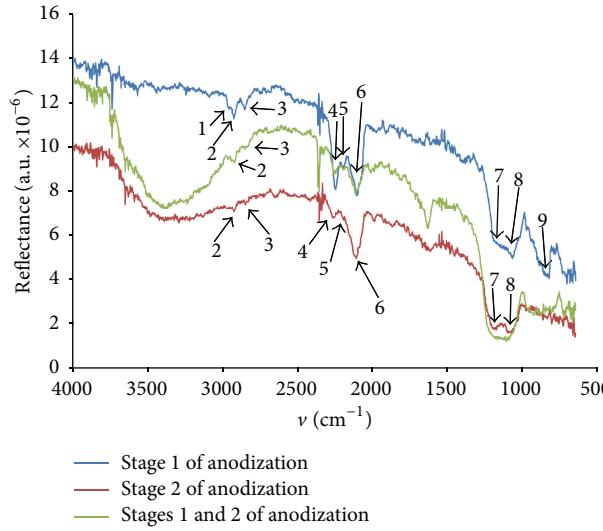

Figure 4: IR spectra of por-Si layers prepared straight before the characterization in the following conditions: the blue color: single-stage syntheses: $j = 80\,\text{mA/cm}^2$, $t = 30\,\text{min}$; the red color: $j = 30\,\text{mA/cm}^2$, $t = 60\,\text{min}$; the green color: two-stage synthesis, series III: stage 1: $j = 80\,\text{mA/cm}^2$, $t = 30\,\text{min}$; stage 2: $j = 30\,\text{mA/cm}^2$, $t = 60\,\text{min}$.

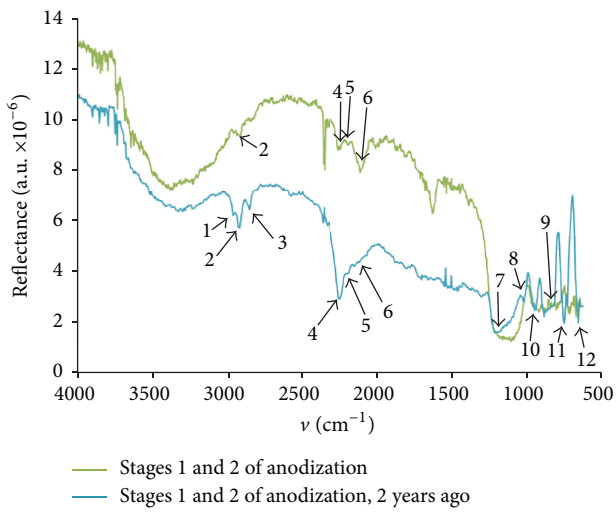

Figure 5: IR spectra of por-Si layers prepared by two-stage process straight before the characterization (green line) and stored within 2 years after the synthesis in the same conditions (blue line).

por-Si surface. A long time storage also led to the increase of bands 1–3 relating to carbon-containing complexes while the band at 3600–$3200\,\text{cm}^{-1}$ decreased (as shown by the increased reflection in this region). The reduced absorption relating to O–H groups in this region can be attributed to the interaction of hydroxyls with alcohol-containing residues of the electrolyte and products of electrochemical oxidation of alcohols diffusing to the surface and forming carbon-containing species. Thus, redistribution of chemical bonds on por-Si surface proceeds in the course of storage. In

Table 2: IR absorption peaks in the por-Si samples interpreted according to [29, 37–39].

Number*	Band position, cm^{-1}	Interpretation
1	2958	Antisymmetric stretching vibrations of CH– in CH_3
2	2927	Antisymmetric stretching vibrations of CH– in CH_2
3	2856	Antisymmetric stretching vibrations of CH– in CH
4	2250	SiH– in O_3–SiH
5	2190	SiH– in SiO_2–SiH
6	2106	SiH– in Si_2H–SiH
7-8	1056–1160	Antisymmetric stretching vibrations of SiO– in O–SiO and C–SiO
9	827	Symmetric stretching vibrations of SiO in O–Si–O
10	948	SiH– in Si_2–H–SiH
11	760	Si–C
12	664	SiH– deformation vibrations

*It corresponds to the relating numbers of absorption bands in Figures 4 and 5.

Table 3: Data of por-Si surface characterization by the adsorption of acid-base indicators with different pK_a values.

pK_a	Indicator	Supposed type of surface centers	Content of surface centers, nmole/cm^2 (on both sides of ~1 × 1 cm plates)	
			Series I Anodization current density 30 mA/cm^2, more uniform surface	Series II Anodization current density 80 mA/cm^2, less uniform surface
2.5	m-Nitroaniline	Acidic hydroxyls ≡Si–OH	28,5	25,2
6.4	Bromocresol purple	Almost neutral hydroxyls $=Si(OH)_2$	7,24	24,9
8.8	Thymol blue	Basic hydroxyls $–Si(OH)_3$	1,17	10,1
14.2	Ethylene glycol	Si atoms	6,1	356

contrast with the fresh por-Si, the samples subjected to a 2-year ageing are featured with a growing surface passivation with hydrogen as indicated by the appearance of bands at 948 cm^{-1} (SiH– in Si_2–H–SiH) and 644 cm^{-1} (SiH pendulum oscillations). It should be also noted that IR reflectance spectrum of por-Si after 2-year storage is more complicated in the region 1000–600 cm^{-1} compared with the same material straight after the synthesis.

3.3. Indicator Adsorption Data on the Surface Functional Composition. A detailed analysis of the surface functional composition using the selective adsorption of acid-base indicators with different pK_a values was carried out for hydrophilic por-Si layers obtained at two different anodization current values (series I and II). The results summarized in Table 3 indicate that the surface of samples prepared at the current density 30 mA/cm^2 is predominantly occupied with Bronsted acidic centers with pK_a 2.5 corresponding to ≡Si–OH groups. The increase of current density to 80 mA/cm^2 results in a drastic decrease in the content of these centers (in agreement with the observed decrease of hydrophilicity) and prevailing of Lewis acidic centers with pK_a 14.2 probably formed by silicon atoms, in combination with a certain increase in the concentration of Bronsted neutral (pK_a 6.4) and basic (pK_a 8.8) centers likely relating to $=Si(OH)_2$ and $–Si(OH)_3$ groups, respectively. Probably the synthesis performed in more "severe" conditions with a significantly higher current density results in "loosening" of the surface layer with multiple disruption of bonds to form versatile centers, including surface silicon atoms as well as "double" and "triple" hydroxyl groups.

4. Conclusions

Porous silicon layers are prepared by single- and two-stage anodization of monocrystalline n-type silicon (111) with the variation of anodization current density, number of synthesis stages, and their conditions as well as storage time after the preparation.

IR reflectance spectroscopy revealed the presence of absorption bands at 2958, 2927, and 2856 cm^{-1} indicating the presence of carbon-containing complexes on por-Si surface with the content of these species depending on the synthesis conditions. A broad absorption band corresponding to surface hydroxyls (O–H bonds) is also observed in the region 3100–3700 cm^{-1}.

The surface of obtained por-Si samples is found to possess hydrophilic properties (as suggested by the absence of bands at 948 and 644 cm^{-1} intrinsic to Si–H bonds in the spectra of samples straight after preparation) mostly prominent in the case of anodization current density 30 mA/cm^2.

The characterization of the prepared por-Si samples by adsorption of acid-base indicators with different pK_a values indicated a possibility for the control over their surface functional composition via the variation of the synthesis conditions. The surface of samples obtained at anodization current density 30 mA/cm^2 is predominantly occupied with pK_a 2.5 corresponding to ≡Si–OH groups. The increase of current density to 80 mA/cm^2 results in the increase of surface functional nonuniformity with the formation of versatile centers, primarily Lewis acidic sites corresponding to Si atoms, as indicated by selective indicator adsorption in agreement with the disappearance of Si–H bonds in IR spectra and overall disordering of the surface morphology according to REM and AFM data.

Generally, the obtained results demonstrate an approach to a wide range adjustment of por-Si porosity and surface properties to address various specific goals.

Competing Interests

The authors declare that there are no competing interests regarding the publication of this paper.

Acknowledgments

This study was supported by the Ministry of Education and Science of the Russian Federation within the framework of the project part of the state assignment for the St. Petersburg Electrotechnical University "LETI" (Project no. 16.2112.2014/K, Preparation and Study of Porous Systems, Functionalized Nanomaterials, Applications in Photonics, Sensor Technology and Medicine).

References

[1] R. J. Martín-Palma, M. Manso-Silván, and V. Torres-Costa, "Biomedical applications of nanostructured porous silicon: a review," *Journal of Nanophotonics*, vol. 4, no. 1, Article ID 042502, 2010.

[2] B. Gupta, Y. Zhu, B. Guan, P. J. Reece, and J. J. Gooding, "Functionalised porous silicon as a biosensor: emphasis on monitoring cells in vivo and in vitro," *Analyst*, vol. 138, no. 13, pp. 3593–3615, 2013.

[3] T. J. Barnes, K. L. Jarvis, and C. A. Prestidge, "Recent advances in porous silicon technology for drug delivery," *Therapeutic Delivery*, vol. 4, no. 7, pp. 811–823, 2013.

[4] V. Y. Shevchenko and O. I. Kiselev, Eds., *Chemical, Biological and Medical Aspects of the Synthesis and Application of Porous Nanocontainers for Drugs*, Handbook, Nauka, Saint-Petersburg, Russia, 2015 (Russian).

[5] J. Rytkönen, R. Miettinen, M. Kaasalainen, V.-P. Lehto, J. Salonen, and A. Närvänen, "Functionalization of mesoporous silicon nanoparticles for targeting and bioimaging purposes," *Journal of Nanomaterials*, vol. 2012, Article ID 896562, 9 pages, 2012.

[6] D. Liu, L. M. Bimbo, E. Mäkilä et al., "Co-delivery of a hydrophobic small molecule and a hydrophilic peptide by porous silicon nanoparticles," *Journal of Controlled Release*, vol. 170, no. 2, pp. 268–278, 2013.

[7] E. Secret, K. Smith, V. Dubljevic et al., "Antibody-functionalized porous silicon nanoparticles for vectorization of hydrophobic drugs," *Advanced Healthcare Materials*, vol. 2, no. 5, pp. 718–727, 2013.

[8] W. Xu, J. Riikonen, and V.-P. Lehto, "Mesoporous systems for poorly soluble drugs," *International Journal of Pharmaceutics*, vol. 453, no. 1, pp. 181–197, 2013.

[9] E. J. Anglin, L. Cheng, W. R. Freeman, and M. J. Sailor, "Porous silicon in drug delivery devices and materials," *Advanced Drug Delivery Reviews*, vol. 60, no. 11, pp. 1266–1277, 2008.

[10] J. L. Coffer, M. A. Whitehead, D. K. Nagesha et al., "Porous silicon-based scaffolds for tissue engineering and other biomedical applications," *Physica Status Solidi (A)*, vol. 202, no. 8, pp. 1451–1455, 2005.

[11] H. A. Santos, L. M. Bimbo, B. Herranz, M.-A. Shahbazi, J. Hirvonen, and J. Salonen, "Nanostructured porous silicon in preclinical imaging: moving from bench to bedside," *Journal of Materials Research*, vol. 28, no. 2, pp. 152–164, 2013.

[12] R.-X. Liu, L.-L. Chen, H.-Y. Zhang, and Z.-H. Jia, "A label-free single photonic quantum well biosensor based on porous silicon for DNA detection," *Optoelectronics Letters*, vol. 9, no. 3, pp. 225–228, 2013.

[13] L. M. Bimbo, O. V. Denisova, E. Mäkilä et al., "Inhibition of influenza A virus infection in vitro by saliphenylhalamide-loaded porous silicon nanoparticles," *ACS Nano*, vol. 7, no. 8, pp. 6884–6893, 2013.

[14] C. J. Shearer, F. J. Harding, M. J. Sweetman, J. G. Shapter, and N. H. Voelcker, "Nanostructured biointerfaces created from carbon nanotube patterned porous silicon films," *Surface and Coatings Technology*, vol. 224, pp. 49–56, 2013.

[15] S. B.-T. de-Leon, R. Oren, M. E. Spira, N. Korbakov, S. Yitzchaik, and A. Sa'ar, "Porous silicon substrates for neurons culturing and bio-photonic sensing," *Physica Status Solidi (A): Applications and Materials Science*, vol. 202, no. 8, pp. 1456–1461, 2005.

[16] A. Yurt, G. G. Daaboul, J. H. Connor, B. B. Goldberg, and M. Selim Ünlü, "Single nanoparticle detectors for biological applications," *Nanoscale*, vol. 4, no. 3, pp. 715–726, 2012.

[17] Y. Shang, W. Zhao, E. Xu, C. Tong, and J. Wu, "FTRIFS biosensor based on double layer porous silicon as a LC detector for target molecule screening from complex samples," *Biosensors and Bioelectronics*, vol. 25, no. 5, pp. 1056–1063, 2010.

[18] A. M. Noval, V. S. Vaquero, E. P. Quijorna et al., "Aging of porous silicon in physiological conditions: cell adhesion modes on scaled 1D micropatterns," *Journal of Biomedical Materials Research A*, vol. 100, no. 6, pp. 1615–1622, 2012.

[19] E. Punzón-Quijorna, V. Sánchez-Vaquero, Á. Muñoz-Noval et al., "Nanostructured porous silicon micropatterns as a tool for substrate-conditioned cell research," *Nanoscale Research Letters*, vol. 7, article 396, 2012.

[20] Y. M. Spivak, A. O. Belorus, P. A. Somov, S. S. Tulenin, K. A. Bespalova, and V. A. Moshnikov, "Porous silicon nanoparticles for target drag delivery: structure and morphology," *Journal of Physics: Conference Series*, vol. 643, no. 1, Article ID 012022, 2015.

[21] A. S. Lenshin, V. M. Kashkarov, Y. M. Spivak, and V. A. Moshnikov, "Investigations of nanoreactors on the basis of p-type porous silicon: electron structure and phase composition," *Materials Chemistry and Physics*, vol. 135, no. 2-3, pp. 293–297, 2012.

[22] L. T. Canham, "Bioactive silicon structure fabrication through nanoetching techniques," *Advanced Materials*, vol. 7, no. 12, pp. 1033–1037, 1995.

[23] C. A. Prestidge, T. J. Barnes, C.-H. Lau, C. Barnett, A. Loni, and L. Canham, "Mesoporous silicon: a platform for the delivery of therapeutics," *Expert Opinion on Drug Delivery*, vol. 4, no. 2, pp. 101–110, 2007.

[24] B. Unal, "Quenching influence of cell culture medium on photoluminescence and morphological structure of porous silicon," *Applied Surface Science*, vol. 258, no. 1, pp. 207–211, 2011.

[25] K. Kimoto and T. Arai, "Photoluminescence of rapid thermal treated porous Si in nitrogen atmosphere," *Physica Status Solidi (A)*, vol. 182, no. 1, pp. 133–137, 2000.

[26] V. Morazzani, J. L. Cantin, C. Ortega et al., "Thermal nitridation of p-type porous silicon in ammonia," *Thin Solid Films*, vol. 276, no. 1-2, pp. 32–35, 1996.

[27] L. M. Bimbo, O. V. Denisova, and E. Mäkilä, "Inhibition of influenza a virus infection in vitro by saliphenylhalamide-loaded porous silicon nanoparticles," *ACS Nano*, vol. 7, no. 8, pp. 6884–6893, 2013.

[28] A. O. Belorus, E. V. Maraeva, Y. M. Spivak, and V. A. Moshnikov, "The study of porous silicon powders by capillary condensation," *Journal of Physics: Conference Series*, vol. 586, no. 1, Article ID 012017, 2015.

[29] A. S. Lenshin, V. M. Kashkarov, P. V. Seredin, Y. M. Spivak, and V. A. Moshnikov, "XANES and IR spectroscopy study of the electronic structure and chemical composition of porous silicon on n- and p-type substrates," *Semiconductors*, vol. 45, no. 9, pp. 1183–1188, 2011.

[30] A. S. Len'shin, V. M. Kashkarov, Y. M. Spivak, and V. A. Moshnikov, "Study of electronic structure and phase composition of porous silicon," *Glass Physics and Chemistry*, vol. 38, no. 3, pp. 315–321, 2012.

[31] I. V. Vasil'eva, S. V. Myakin, E. V. Rylova, and V. G. Korsakov, "Electron-beam modification of the surface of oxide materials (SiO_2 and $BaTiO_3$)," *Russian Journal of Physical Chemistry*, vol. 76, no. 1, pp. 71–76, 2002.

[32] S. V. Mjakin, M. M. Sychov, and I. V. Vasilieva, Eds., *Electron Beam Modification of Functional Materials*, Petersburg State Transport University, Saint-Petersburg, Russia, 2006.

[33] K. Imai and H. Unno, "FIPOS technology and its application to LSI's," *IEEE Transactions on Electron Devices*, vol. 31, pp. 297–302, 1984.

[34] H. Föll, M. Christophersen, J. Carstensen, and G. Hasse, "Formation and application of porous silicon," *Materials Science and Engineering R: Reports*, vol. 39, no. 4, pp. 93–142, 2002.

[35] M. F. Panov and V. V. Tomaev, "Optical reflection of oxidized PbSe films in the infrared spectral range," *Glass Physics and Chemistry*, vol. 38, no. 4, pp. 419–426, 2012.

[36] A. A. Kopylov and A. N. Kholodilov, "Infrared absorption in porous silicon obtained in electrolytes containing ethanol," *Semiconductors*, vol. 31, no. 5, pp. 470–472, 1997.

[37] A. Borghesi, A. Sassella, B. Pivac, and L. Pavesi, "Characterization of porous silicon inhomogeneities by high spatial resolution infrared spectroscopy," *Solid State Communications*, vol. 87, no. 1, pp. 1–4, 1993.

[38] A. Borghesi, G. Guizzetti, A. Sassella, O. Bisi, and L. Pavesi, "Induction-model analysis of SiH stretching mode in porous silicon," *Solid State Communications*, vol. 89, no. 7, pp. 615–618, 1994.

[39] V. P. Tolstoy, I. V. Chernyshova, and V. A. Skryshevsky, *Handbook of Infrared Spectroscopy of Ultrathin Films*, Wiley Interscience, 2003.